Bond between near-surface mounted CFRP laminates and the concrete in structural strengthening

J. Sena Cruz & J. Barros
Dep. of Civil Engineering, University of Minho, Campus de Azurém, 4800-058 Guimarães, Portugal

ABSTRACT: Near Surface Mounted (NSM) Laminate Strips of Carbon Fiber Reinforced Polymer (LS-CFRP) is a promising technique for increasing the flexural and shear strength of deficient reinforced concrete members. When compared to externally bonded reinforcing (EBR) technique, NSM LS-CFRP technique shows several advantages, namely: higher prevention to the peeling phenomenon; extra protection against fire, mechanical and environmental damaging effects; easier and faster installation. To evaluate the concrete/LS-CFRP bond behavior, an experimental campaign of pullout-bending tests was carried out, where the influence of the concrete strength and the LS-CFRP bond length was considered. Taking the experimental results and using a numerical method developed for this purpose, an analytical bond stress-slip relationship was evaluated. The present paper describes the numerical strategy developed, its applicability to the tests carried out and its usefulness for predicting the anchorage length.

1 INTRODUTION

Since 1999, a strengthening technique based on the Near Surface Mounted (NSM) of Laminate Strips of Carbon Fiber Reinforced Polymer (LS-CFRP) has been used for increasing the load bearing capacity of concrete members.

In this strengthening technique the LS-CFRP are introduced into grooves made on the concrete cover of the elements to be strengthened that were previously filled with epoxy adhesive. The LS-CFRP has a cross section of about 1.4 mm thick and 10 mm width. The width and the depth of the groove vary between 3 and 5 mm, and between 12 to 15 mm, respectively.

To evaluate the efficiency of the NSM LS-CFRP technique concrete columns (Barros et al. 2001) and concrete beams (Barros & Fortes 2002) were strengthened for increasing their bending capacity, and concrete beams were strengthened to increase their shear capacity (Dias & Barros 2003). The results proved that this technique is more effective than externally bonded reinforcing (EBR) technique because higher stresses on the LS-CFRP can be mobilized at the failure of the strengthened elements, larger deformations can be attained, and higher resistance to peeling phenomenon is assured.

To characterize the bond behavior of the LS-CFRP to concrete, pullout-bending tests were carried out (Sena-Cruz & Barros 2002a, b). The pullout force at the LS-CFRP, and the slip at the free and loaded ends were measured. The influence of the concrete strength and bond length on the bonding behavior of these two materials was analyzed. From the results obtained, it can be pointed out the following remarks:

- The failure occurred by pullout of the LS-CFRP;
- The peak pullout force and the corresponding slip increased with the bond length;
- The bond strength revealed a tendency to decrease with the increase of the bond length;
- The bond strength attained values significantly higher than the ones obtained using externally bonded CFRP and NSM FRP rods reinforcing techniques (De Lorenzis 2002);
- The influence of the concrete strength on the main parameters analyzed was marginal;
- The evolution of the bond stress and the slip along the bond length is essentially nonlinear.

The results obtained from the experiments were used in a numerical model to define a local bond stress-slip relationship, which takes into account the distribution of the slip and the bond stress along the LS-CFRP. The numerical method developed is described and a local bond stress-slip relationship for NSM LS-CFRP strengthening technique is proposed.

2 DIFFERENTIAL EQUATION

Assuming that LS-CFRP has a linear-elastic behavior and neglecting the thickness of this composite material, the equilibrium of a LS-CFRP of length *dx* bonded to concrete can be given by the following expression (see Figs 1-2):

$$\tau(x) = \frac{E_f t_f}{2} \frac{d\varepsilon_f}{dx} \tag{1}$$

where $\tau(x)$ is the bond stress acting on the contact surface between LS-CFRP and epoxy-adhesive, E_f, t_f and ε_f are the Young's modulus, the thickness and the strain of the LS-CFRP, respectively.

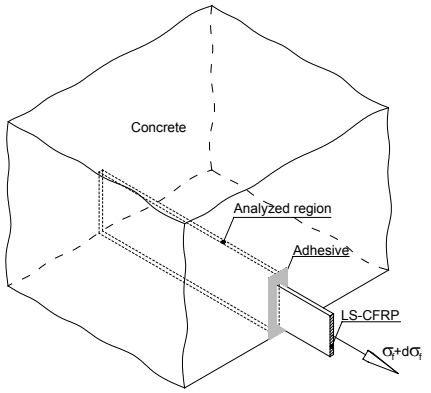

Figure 1. Region of interest in the analysis.

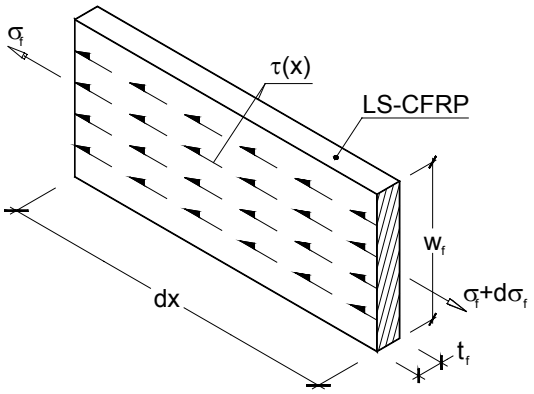

Figure 2. Equilibrium of the LS-CFRP.

In a representative region of the (LS-CFRP)-adhesive-concrete bonding, the strain components indicated in Figure 3 are presented. Neglecting the concrete and the adhesive deformability on the slip evaluation, the LS-CFRP strain can be obtained from the slip variation, *ds*:

$$\varepsilon_f = \frac{ds}{dx}. \tag{2}$$

Replacing Equation 2 into Equation 1, the differential equation that governs the slip of LS-CFRP bonded into concrete is derived:

$$\frac{d^2 s}{dx^2} = \frac{2}{t_f E_f} \tau(s). \tag{3}$$

Based on expressions similar to this one, important phenomenon's of concrete behavior, like, reinforcement anchorage length, tension-stiffening, crack spacing and crack opening, can be simulated. The quality of the local bond-slip relationship, $\tau(s)$, has decisive importance on the accuracy of this simulation.

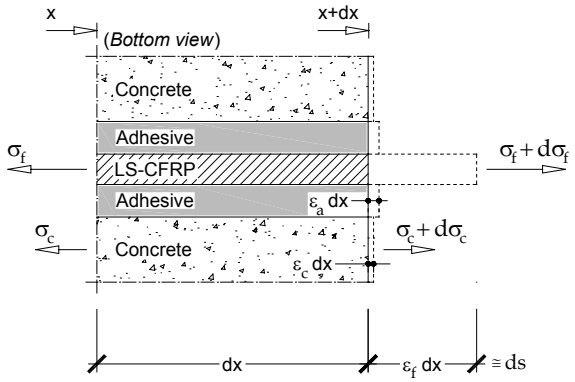

Figure 3. Strain of the intervening materials of the bond region.

3 METHOD TO FIND THE LOCAL BOND-STRESS SLIP RELATIONSHIP

The method adopted to determine the local bond stress-slip law, $\tau = \tau(s)$, was based on the work developed by Focacci et al. (2000). Adjustments were implemented to take into account the specificities of the present strengthening technique.

3.1 *Analytical expressions for local bond-stress slip relationship*

Based on the methodology used on the bonding of steel bars to concrete, several approaches have been developed to establish the $\tau = \tau(s)$ relationship for FRP rods (Larralde et al. 1993, Malvar 1995, Cosenza et al. 1997, Focacci et al. 2000, De Lorenzis et al. 2002).

In the present work the local bond stress-slip relationship is composed by the following two equations:

$$\tau(s) = \begin{cases} \tau_m \times \left(\frac{s}{s_m}\right)^{\alpha} & if \quad s \le s_m \\ \tau_m \times \left(\frac{s}{s_m}\right)^{-\alpha'} & if \quad s > s_m \end{cases} \tag{4}$$

where τ_m and s_m are the bond strength and its corresponding slip, and α and α' are parameters defin-

ing the shape of the curves. The equation for $s \le s_m$ was used by Eligehausen et al. (1983) and defines the bond behavior up to peak stress (ascending branch). The equation for $s > s_m$ was adopted by De Lorenzis et al. (2002) and reproduces the post-peak bond behavior (descending branch). This law was selected due to its simplicity and ability to simulate the phenomena under discussion

3.2 *Notation adopted*

Figure 4 represents a LS-CFRP, fixed to concrete by epoxy-adhesive on a bond length (L_b). If the LS-CFRP is slipping due to a pullout force applied, $\overline{N}$, the slip, $s = s(x)$, the bond stress between the LS-CFRP and the epoxy-adhesive, $\tau = \tau(x)$, the strain on the LS-CFRP, $\varepsilon = \varepsilon_f(x)$, and the axial force on LS-CFRP, $N = N(x)$, along the bond length can be obtained. For the particular case of the bond length extremities, designated by loaded end and free end:

$$x = 0 \Rightarrow \begin{cases} s = s_f \\ N = 0 \\ \varepsilon_f = 0 \end{cases} ; \; x = L_b \Rightarrow \begin{cases} s = s_l \\ N = \overline{N} \\ \varepsilon_f = \overline{N} / \left(E_f \times A_f \right) \end{cases} \quad (5)$$

where s_f and s_l are the slips at free and loaded ends, respectively. In the present work, numerical and experimental entities will be involved, having been differentiated by a strikeover on the experimental ones. For instance, $\overline{N}_i$ represents the pullout force experimentally measured in the *i*-th scan reading.

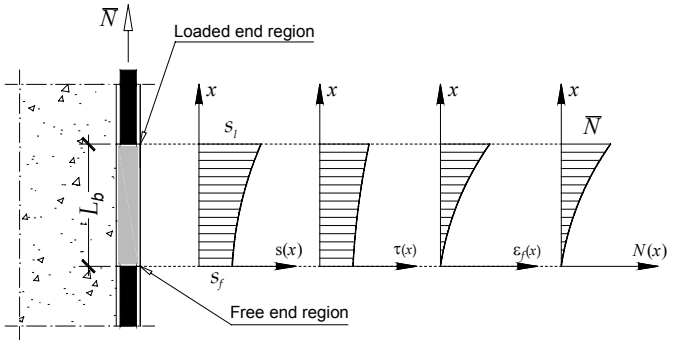

Figure 4. Functions involved.

3.3 *Description of the method*

From the pullout bending tests carried out, the slip at the free end, $\overline{s}_f$, the slip at the loaded end, $\overline{s}_l$, and the pullout force, $\overline{N}$, were obtained. For a generic scan reading *i*, the $\overline{s}_f^i$, $\overline{s}_l^i$ e $\overline{N}_i$ were known. Using these experimental results, the purpose was obtain the parameters s_m, τ_m, α and α' of Equation 4 that fit the differential Equation 3 as much as possible.

To get such aim, a computational code was developed (in ANSI-C language, using some concepts of the C++ language), based on the algorithm described in Figure 5.

In this algorithm the second order differential Equation 3 needs to be solved. The Runge-Kutta-Nyström (RKN) (Kreyszig 1993) method was used for this purpose.

This algorithm is composed by the following main steps:

- *Defining the local bond stress-slip relationship*: in the first step the parameters s_m, τ_m, α and α' are fixed, in order to define the $\tau = \tau(s)$ relationship and its error;
- *Determination of the $\widetilde{s}_l$ parameter*: evaluation of the maximum loaded end slip, when the free end slip does not occur (see *Module A*);
- *Read the experimental values*: for the experimental *i*-th scan reading, the free end slip, $\overline{s}_f^i$, the loaded end slip, $\overline{s}_l^i$ and the pullout force, $\overline{N}_i$ are read;
- *Calculate the pullout force* $N_i\left(\overline{s}_f^i\right)$: taking the free end slip, $\overline{s}_f^i$, and using Equation 3, the numerical pullout force at the loaded end, $N_i\left(\overline{s}_f^i\right)$, is calculated (see *Module B*);
- *Calculate the error associated to* $N_i\left(\overline{s}_f^i\right)$: the error was the difference, in absolute value, between the areas corresponding to the experimental and numerical curves. The points $\left(\overline{s}_f^{i-1}, N_{i-1}\left(\overline{s}_f^{i-1}\right)\right)$ and $\left(\overline{s}_f^i, N_i\left(\overline{s}_f^i\right)\right)$ were used for defining the numerical curve, while experimental curve was defined from points $\left(\overline{s}_f^{i-1}, \overline{N}_{i-1}\right)$ and $\left(\overline{s}_f^i, \overline{N}_i\right)$;
- *Calculate the pullout force* $N_i\left(\overline{s}_l^i\right)$: taking the loaded end slip, $\overline{s}_l^i$, and using Equation 3 the pullout force at the loaded end, $N_i\left(\overline{s}_l^i\right)$, is evaluated. However, in this case the following two loaded end slip conditions should be considered: i) if $\overline{s}_l^i < \widetilde{s}_l$ the determination of $N_i\left(\overline{s}_l^i\right)$ must take into account that the effective bond length is less than L_b (see *Module C*); ii) if $\overline{s}_l^i \ge \widetilde{s}_l$ the evaluation of $N_i\left(\overline{s}_l^i\right)$ is based on the *Module D*;
- *Calculate the error associated to* $N_i\left(\overline{s}_l^i\right)$: the error was the difference, in absolute value, between the areas corresponding to the experimental and numerical curves. The points $\left(\overline{s}_l^{i-1}, N_{i-1}\left(\overline{s}_l^{i-1}\right)\right)$ and $\left(\overline{s}_l^i, N_i\left(\overline{s}_l^i\right)\right)$ were used for defining the numerical curve, while experimental curve was defined from points $\left(\overline{s}_l^{i-1}, \overline{N}_{i-1}\right)$ and $\left(\overline{s}_l^i, \overline{N}_i\right)$.

In the *Modules C* and *D* an iterative method is required. In the present work the method of the successive bisection was used.

4 EXAMPLE

Beam *B2_fcm45_La80*, of the pullout bending tests carried out by Sena-Cruz & Barros (2002a), was selected to exemplify the application of the method described in the last section.

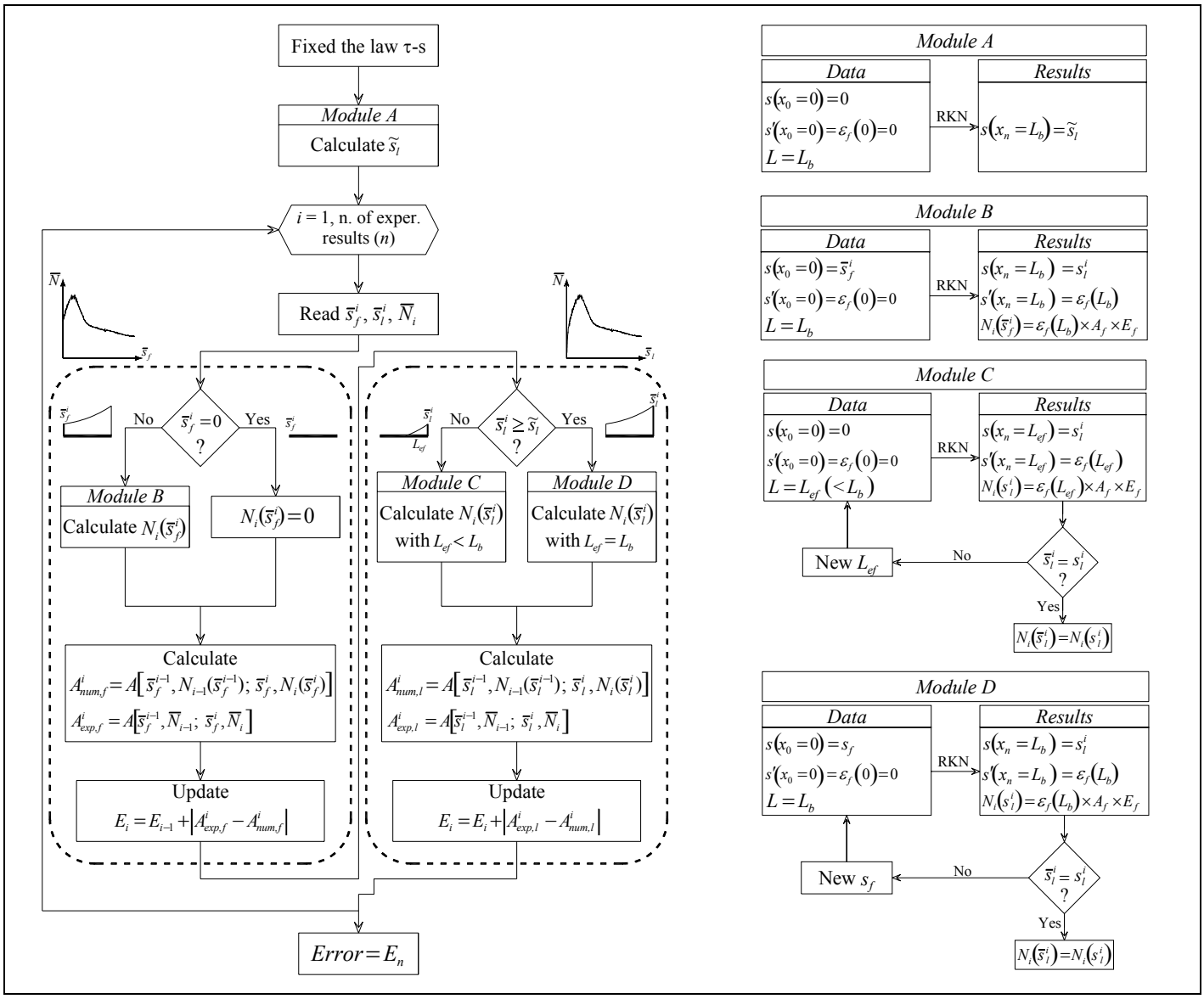

Figure 5. Algorithm implemented.

The average concrete compression strength and the bond length of this specimen are 45 MPa (f_{cm}) and 80 mm ($= L_b$), respectively. The LS-CFRP had $t_f = 1.39$ mm and $E_f = 160$ GPa.

To assure that peak pullout force and its corresponding slip obtained numerically were similar (less than a tolerance of 1%) to the values registered experimentally, the following method was used:

- *Step 1*: fixing the parameters α and α', the parameters s_m and τ_m of the best fitting were found;
- *Step 2*: using the parameters s_m and τ_m obtained in the previous step, the parameters α and α' giving the better fitting were determined.

To assure the tolerance imposed, some cases required the use of an iterative procedure on these steps.

The performance of the method developed is well demonstrated in Figure 6, where the experimental and the numerical slip-pullout force relationship are compared. At the peak pullout load, the evolution of the slip, bond stress and axial force along the bond length is shown in Figure 7. At this loading phase the bond behavior is essentially nonlinear, and half of bond length is in the softening regime.

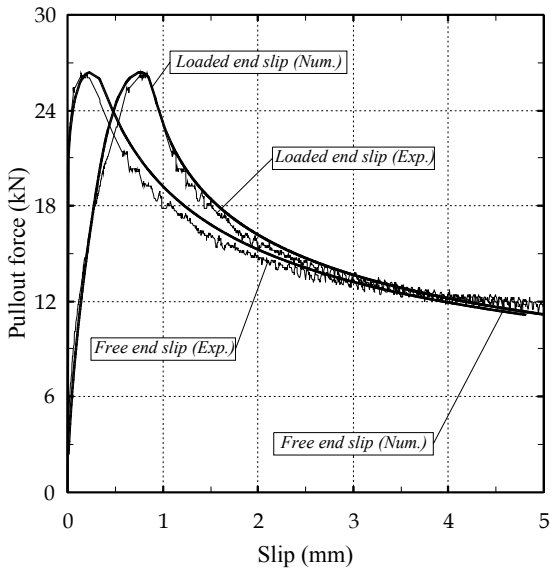

Figure 6. Simulation of specimen *B2_fcm45_La80.*

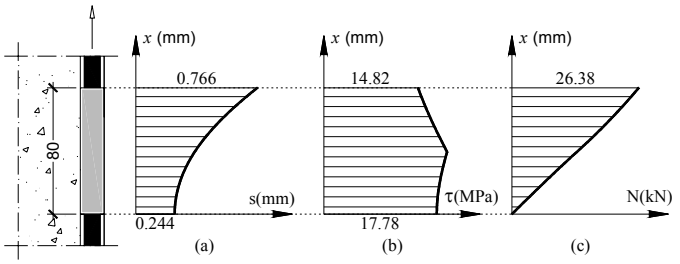

Figure 7. Evolution of the slip (a), bond stress (b) and axial force (c) along the bond length of specimen *B2_fcm45_La80*.

5 LOCAL BOND STRESS-SLIP LAW FOR NSM LS-CFRP TECHNIQUE

Using the results obtained on the experimental campaign (Sena-Cruz & Barros 2002a), the parameters s_m, τ_m, α and α' of the local bond stress-slip law (see Eq. 4) were found using the procedure described in Section 3 and applied in Section 4. For each series (composed by three specimens), the average relationship between the loaded end slip and the pullout force was used to calibrate the law.

Figure 8 shows that the loaded end slip *vs* pullout force relationship obtained numerically (thick line) fits quite well the corresponding experimental envelop (hatch). Similar performance was registered on the remainder series.

The values of the parameters' law and the error obtained in the corresponding numerical analysis are included in Table 1. The error is the difference, in absolute value, between the areas corresponding to the experimental and numerical curves. From these data it can be pointed out the following observations:

- the error of each series is quite acceptable;
- a reasonable coefficient of variation was obtained on the average bond strength;
- large scatter on the values s_m, α and α' was obtained;
- a linear increasing trend of s_m with the bond length is observed.

Table 1. Values of the parameters defining the local bond stress-slip relationship.

Series	s_m	τ_m	α	α'	Error
	mm	MPa			%
_fcm35_La40	0.180	20.60	0.13	-0.27	2.04
_fcm35_La60	0.228	20.68	0.19	-0.35	5.92
_fcm35_La80	0.290	18.90	0.17	-0.33	6.96
_fcm45_La40	0.144	21.40	0.21	-0.23	4.66
_fcm45_La60	0.231	19.50	0.24	-0.39	2.98
_fcm45_La80	0.430	19.50	0.35	-0.45	2.75
_fcm70_La40	0.189	21.50	0.24	-0.29	7.82
_fcm70_La60	0.210	18.00	0.21	-0.29	3.37
_fcm70_La80	0.345	18.20	0.19	-0.27	2.36
Average	0.250	19.81	0.21	-0.32	–
C.V. (%)*	36.19	6.60	29.05	21.49	–

*Coefficient of variation

6 ANCHORAGE LENGTH

Due to safety and economical reasons, the anchorage length L_{an} of the LS-CFRP should be evaluated for accomplishing the requisites imposed by service and ultimate limit state analysis, i.e.:

$$L_{an} = \max\left\{L_{an,S}, L_{an,U}\right\} \tag{6}$$

where $L_{an,S}$ and $L_{an,U}$ are the anchorage length at service and ultimate limit states, respectively.

To determine the anchorage length, the local bond stress-slip should be known. In the present analysis the average values of τ_m, α and α' were used (see Tab. 1), and s_m was considered as linearly dependent of L_b ($s_m = 0.0042 \times L_b$).

At service limit state it is desired that the free end does not slip (Focacci et al. 2000, De Lorenzis et al. 2002), consequently, the pullout force at the onset of free end slip is of practical interest. According to the method described in Section 3.3, this pullout force corresponds to $N(\widetilde{s}_l)$. Figure 9 includes the $N(\widetilde{s}_l)$ as a function of the bond length. The experimental results are also included (donuts). Using this diagram, it is possible to find the bond length, $L_{an,S}$, for a given pullout service load.

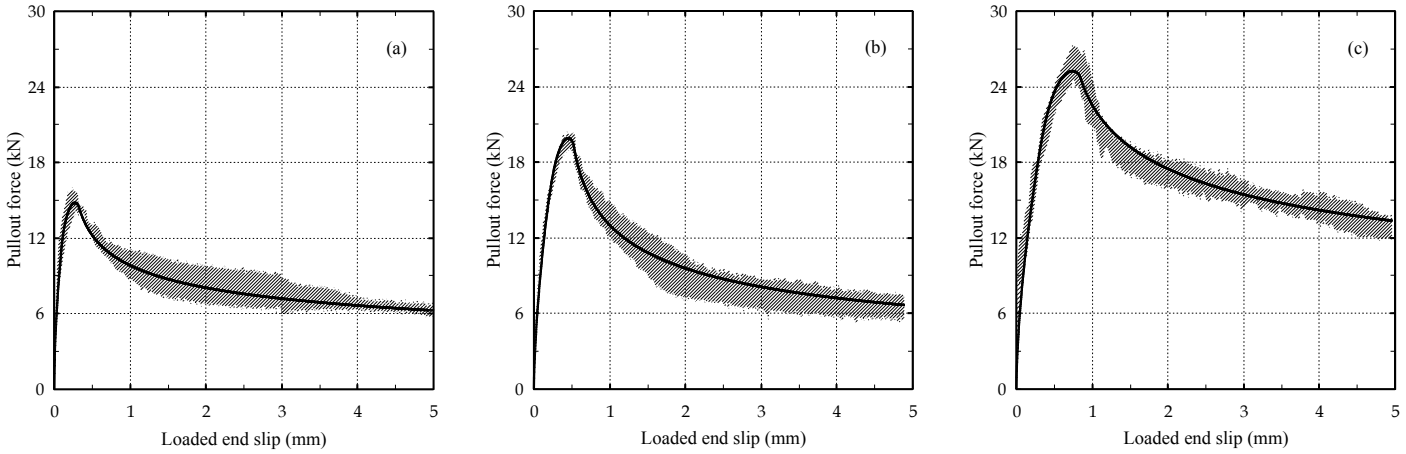

Figure 8. Numerical and experimental results on series *_fcm35_La40* (a), *_fcm45_La60* (b) and *_fcm70_La80*.

To predict the failure, the entire bond stress-law relationship should be known (see Fig. 7). Figure 10 relates the pullout load with the bond length, for the determination of $L_{an,U}$. A good fit can be observed between experimental and numerical results. This graph can be used to evaluate the $L_{an,U}$ for a pullout force obtained from an ultimate limit state.

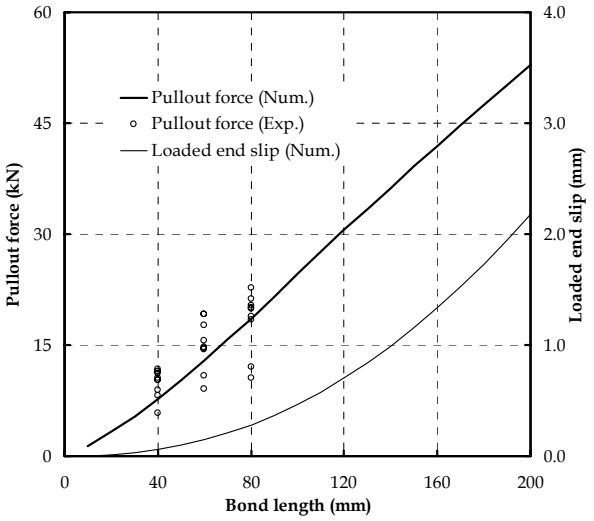

Figure 9. Relationship between the pullout force at the onset of free end slip and the bond length.

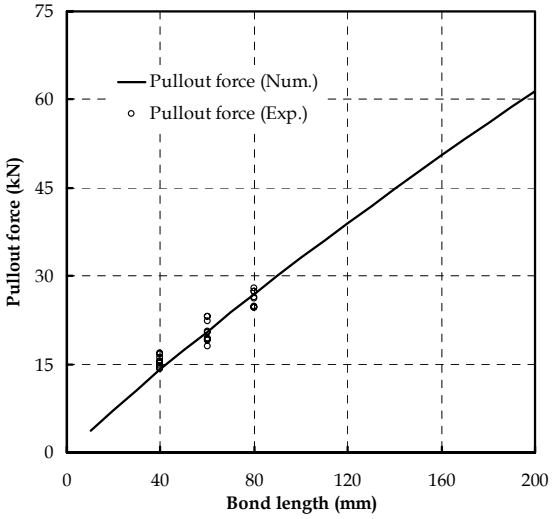

Figure 10. Relationship between the pullout load and the bond length.

7 CONCLUSIONS

A numerical method to calibrate the parameters that define a local bond stress-slip relationship for NSM LS-CFRP technique was developed. The numerical strategy involved the data obtained on experimental tests and the numerical solution of the second-order differential equation that governs the slipping phenomenon. The local bond stress-slip law evaluated from this strategy can predict with enough accuracy the bond behavior registered experimentally. It was also demonstrated that the method is useful for determining the anchorage length of LS-CFRP for service and ultimate limit state analysis.

8 ACKNOWLEDGEMENTS

The authors wish to acknowledge the fruitful discussion with Dr. Francesco Focacci.

9 REFERENCES

Barros, J.A.O., Fortes, A.S. 2002. Concrete beams reinforced with carbon laminates bonded into slits. 5º Congreso de Métodos Numéricos en Ingeniería, Madrid, 16 pp.

Barros, J.A.O., Sena-Cruz, J.M.S., Ferreira, D.R.S.M., Lourenço, P.J.B. 2001. Análise experimental de pilares de betão armado reforçados com laminados de carbono sob acções cíclicas. 5º Encontro Nacional de Sismologia e Engenharia Sísmica, *Laboratório Regional de Engenharia Civil, Ponta Delgada*, Açores, 491-503.

Cosenza, E., Manfredi, G., and Realfonzo, R. 1997. Behavior and modeling of bond of FRP rebars to concrete. *Journal of Composites for Construction*, *ASCE*, 1(2), 40–51.

De Lorenzis., L. 2002. Strengthening of RC structures with near-surface mounted FRP rods. PhD Dissertation, University of Lecce, Italy.

De Lorenzis, L., Rizzo, A., La Tegola, A. 2002. A modified pull-out test for bond of near-surface mounted FRP rods in concrete. *Elsevier, Composites Part B: Engineering,* Vol. 33, Issue 8, December, 589-603.

Dias, S.J.E.; Barros, J.A.O. 2003. Materias compósitos de CFRP no reforço ao corte de vigas de betão armado (*CFRP materials for shear strengthening of concrete beams*). Paper to be presented in 3º Congresso Luso-Moçambicano de Engenharia. (in Portuguese).

Eligehausen, R., Popov, E.P., and Bertero, V.V. 1983. Local bond stress-slip relationships of deformed bars under generalized excitations. *Report Nº 83/23*, *Envir. Engrg. Res. Council*, University of California, Berkeley, California.

Focacci, F., Nanni, A., Bakis, C.E. 2000. Local bond-slip relationship for FRP reinforcement in concrete. *Journal of Composites for Construction*, *ASCE*, Vol. 4, Nº1, 24-31.

Kreyszig, E. 1993. Advanced engineering mathematics, *John Wiley & Sons*, 7th edition.

Larralde, J., and Silva-Rodriguez, R. 1993. Bond and slip of FRP rebars in concrete. *Journal of Materials in Civil Engineering*, *ASCE*, 5(1), 30–40.

Malvar, L. 1995. Tensile and bond properties of GFRP reinforcing bars. *ACI Material Journal*, 92(3), 276–2985.

Sena-Cruz, J., Barros, J. 2002a. Caracterização experimental da ligação de laminados de CFRP inseridos no betão de recobrimento (*Experimental characterization of CFRP laminates bonded to concrete cover*). Technical Report 02-DEC/E-15, Dep. of Civil Engineering, University of Minho, Portugal, 54 pp. (in portuguese).

Sena-Cruz, J.M.; Barros, J.A.O. 2002b. Bond behavior of carbon laminate strips into concrete by pullout-bending tests. Bond in Concrete – from the research to standards, International Symposium, *FIB*, Budapest, Hungry, November, 614-621.